Paramagnetic resonance and local position of Cr^{3+} in ferroelectric $BaTiO_3$

K. A. Müller and W. Berlinger
IBM Zurich Research Laboratory, 8803 Rüschlikon, Switzerland

J. Albers
Physics Department, Universität des Saarlandes, 6600 Saarbrücken, West Germany
(Received 6 June 1985)

EPR spectra of Cr^{3+}, $S=\frac{3}{2}$, substituting for Ti^{4+} are reported as a function of temperature T in all four phases of $BaTiO_3$. In the three ferroelectric phases (FEP's), the principal axis of the Hamiltonian is always along the polar axis. There are two crystal-field terms, one proportional to the square of the polarization and a large one linear in T. The latter is the *same* in all FEP's. The existence of the first term shows that the Cr^{3+} remains centered in the octahedral cell. The existence of the latter, not observed for Fe^{3+}, points to large thermal fluctuations of the Cr^{3+}. These are ascribed to the absence of antibonding, repelling e_g electrons directed towards the oxygen atoms which are present for Fe^{3+}. Saturation of the $b_2^0(T)$ term for low T is accounted for by a Debye model for Cr^{3+} with an energy of only 236.6 K, proving independently a flat ionic potential for Cr^{3+}. The picture of considerable Cr^{3+} amplitude fluctuations agrees with an effectively reduced Cr^{3+}-O^{2-} distance of 0.02 Å compared to the Fe^{3+}-O^{2-} distance obtained from the superposition-model analysis. The latter yields the correct sign and magnitude of the crystal-field b_2^0 terms in all FEP's. It confirms that a maximum of the intrinsic superposition-model parameter $\overline{b_2}(R)$ for Cr^{3+}, derived earlier by Müller and Berlinger, occurs for R between 1.95 and 1.96 Å.

I. INTRODUCTION

Recently, Siegel and Müller[1] were able to interpret some two-decade-old paramagnetic resonance experiments on Fe^{3+} substituting for Ti^{4+} in $BaTiO_3$. These early experiments of Hornig, Rempel, and Weaver[2] were carried out as a function of temperature in the cubic and tetragonal ferroelectric phases (FEP's). Studies of Sakudo and Unoki[3] extended the investigations to the orthorhombic and rhombohedral phases for one specific temperature in each of the two phases. It was shown in the aforementioned analysis, using the superposition model with parameters determined earlier,[4] that the Fe^{3+} participates by less than an order of magnitude in the collective motion of the Ti^{4+} ions responsible for ferroelectricity, i.e., the Fe^{3+} remains at the center of the oxygen octahedron in all three ferroelectric phases.

The sizes of Ti^{4+} and Fe^{3+} in octahedral oxygen coordination are nearly the same. The difference in behavior, that one undergoes a cooperative transition and the other remains centered, can have two origins. (a) The Ti^{4+} has an empty $3d$ shell, whereas that of the Fe^{3+} is half-filled. It has been discussed that the emptiness of the Ti^{4+} d shell is crucial for the occurrence of the ferroelectricity.[1] (b) There is a charge difference of one unit between Ti^{4+} and Fe^{3+}. In a recent theoretical study, Sangster[5] showed the occurrence of radial enhancement of ions owing to the charge misfit between the substituted ion and the impurity. Thus the radius of Fe^{3+} is enhanced in $BaTiO_3$ as compared to that in an oxide, where it replaces an intrinsic trivalent ion. In order to elucidate further the two possible reasons for the centering of the Fe^{3+} just mentioned, another trivalent ion with nearly the same ionic radius as that of Fe^{3+},[6] but with a different $3d$ configuration, has been studied.

Cr^{3+} is such an ion, but with an electron configuration $3d^3$ as compared to Fe^{3+} with $3d^5$. Whereas Fe^{3+} in the high-spin configuration has its two subshells with t_{2g} and e_g character half-filled, $(t_{2g})^3$,$(e_g)^2$, Cr^{3+} has only the t_{2g} subshell half filled with configuration $(t_{2g})^3$ and the (e_g) shell empty. The $(e_g)^2$ are antibonding σ orbitals and will cause a larger repulsion from the negative oxygen shells to keep the Fe^{3+} centered; see Fig. 1. On the other hand, the $(t_{2g})^3$ are essentially nonbonding, having their charge density pointing midway between the oxygen electron density. Recent uniaxial stress experiments on Cr^{3+} in cubic MgO at room temperature indicated that Cr^{3+} may be slightly off center along the $\langle 100\rangle$ cubic positions.[7] Thus Cr^{3+} appeared as a valid candidate to decide whether the $3d^n$ configuration or the size enhancement, owing to the charge misfit, is more important.

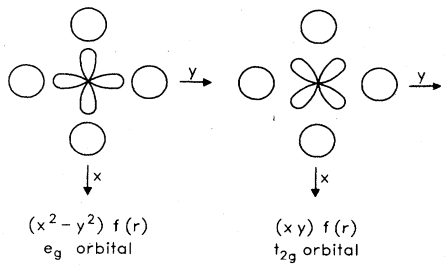

FIG. 1. Shapes of e_g and t_{2g} orbitals in octahedral coordination.

In order to investigate quantitatively the Cr^{3+} position in $BaTiO_3$, a paramagnetic resonance study of Cr^{3+} was carried out in such a doped single crystal. EPR spectra were investigated in all four phases as a function of temperature. The spectra obtained are very *different* from those observed for Fe^{3+} as far as the size of the splittings, their signs, and the orientation of the principal magnetic axis in the orthorhombic phase are concerned. These findings are described in Sec. II.

The main EPR crystal-field term $b_2^0(T) \equiv D(T)$ in the Hamiltonian for the three FEP's between 100 K and the highest T_c at 410 K could be accounted for by just two terms for each phase, one proportional to the square of the lattice polarization $P(T)$ and a large one linear in temperature, the latter being the same for all FEP's. The term proportional to $P^2(T)$ is direct evidence for Cr^{3+} remaining centered. The Cr^{3+} however is barely centered because of the term linear in T which is a result of large local fluctuations; such a linear term is not observed for Fe^{3+}. The Cr^{3+} fluctuations are confirmed by the low-temperature behavior of $D(T)$ between 4.2 and 100 K which can be accounted for by a Debye model for Cr^{3+} with quite a low oscillator energy of only 236.6 K as compared to that for Fe^{3+} in $BaTiO_3$ with a Debye temperature of $\Theta = 450$ K. This part of the analysis is given in Sec. III.

The analysis of the observed b_2^m crystal-field term was rendered possible by the superposition model parameters for Cr^{3+} in the octahedral oxygen position obtained recently by Müller and Berlinger.[7] For that model, the authors computed an intrinsic $\bar{b}_2(R)$ function from uniaxial stress experiments on Cr^{3+} in $SrTiO_3$ and MgO. This function was deduced to be positive and to have a maximum near $R = 1.957$ Å, in contrast to the case for Fe^{3+} where $\bar{b}_2(R)$ is negative with no extremum in that range. The b_2^m terms observed for Cr^{3+} in $BaTiO_3$ are accounted for, as far as the sign and orientation of magnetic axes are concerned. They also prove that the $\bar{b}_2(R)$ function does indeed have a maximum. A satisfactory agreement regarding the magnitude could be reached by assuming the effective Cr^{3+}-O^{2-} distance is reduced by 0.02 Å from the intrinsic six oxygen positions towards the center. This can be regarded as a consequence of the large Cr^{3+} ionic fluctuation towards the oxygen atoms, absent for Fe^{3+}. Thus the absence of e_g electrons for Cr^{3+} in $BaTiO_3$ does indeed render the potential considerably flatter than that for Fe^{3+}, but the charge misfit suffices to keep a potential minimum at the center of the octahedron. This part of the analysis is detailed in Sec. IV followed by a short conclusion in Sec. V.

II. EXPERIMENTS

A. Crystal growth and sample preparation

The Cr-doped $BaTiO_3$ single crystal was pulled from a nonstoichiometric melt by the top-seeded solution technique.[8,9] The raw materials were $BaTiO_3$—obtained by thermal decomposition of barium titanyl oxalate (Merck Selectipur)—and TiO_2 (Merck Optipur) in a ratio of 51 mol % $BaTiO_3$ and 49 mol % TiO_2, with a total weight of 129 g. After the addition of 0.193 g of Cr_2O_3, the materials were melted in a 100-ml platinum crucible at 1400 °C. Single-crystal growth with an undoped $BaTiO_3$ seed was achieved by cooling the melt from 1380 °C to 1320 °C at a rate of about 0.8 °C/h. The crucible was cooled slowly within the oven to room temperature (10 °C/h from 1320 °C to 150 °C, 3 °C/h below 150 °C).

The 12-g crystal could be oriented roughly on an optical goniometer with the aid of its pseudocubic natural faces. Atomic absorption spectroscopy revealed a chromium content of 0.023 ± 0.003 wt % Cr, which is about one-fourth of that present in the melt.

Cylindrically shaped samples with a diameter of 0.7 mm and length of 0.9 mm, were machined from the single-crystal boule with a very fine diamond grinding wheel. While shaping this brittle material, the temperature was kept around ambient temperature to prevent the sample from passing from its tetragonal into the orthorhombic phase. These samples were located with their axes centered along that of the cylindrical cavity of the superheterodyne spectrometer working at 19.2 GHz.[10] Accurate centering minimized the losses in the cavity. The sample cylinder axis was chosen to be a $[1\bar{1}0]$ direction. The external magnetic field could be rotated perpendicularly to this axis, in the $(1\bar{1}0)$ plane. This allowed spectra to be recorded with **H** along the [100], [110], and [111] pseudocubic crystal directions. Such spectra sufficed to evaluate the fine structure of the spin Hamiltonian in all phases of $BaTiO_3$.

B. Cr^{3+} EPR spectra

In the *cubic phase,* an isotropic single EPR line of Cr^{3+}, $S = \frac{3}{2}$, is observed at $g = 1.975 \pm 0.002$. This g value is close to that found for the ion in the octahedral environment of MgO ($g = 1.980$) (Ref. 11) and $SrTiO_3$ ($g = 1.978$),[12] and allows one to conclude that Cr^{3+} is substitutional on the Ti^{4+} lattice site. Below the cubic-to-tetragonal phase transition of $BaTiO_3$ at 282.5 ± 2.5 K, three mutually perpendicular axial spectra appear corresponding to the six tetragonal $\langle 100 \rangle$ ferroelectric domains. Each of these sets can be described by the usual axial spin Hamiltonian,[13]

$$\mathcal{H} = g\beta \mathbf{S} \cdot \mathbf{H} + D_t[S_{z'}^2 - \tfrac{1}{3}S(S+1)] \tag{1}$$

with $\hat{z}' \| \langle 100 \rangle$. Within the accuracy of our experiments, the g value was isotropic. For a magnetic field parallel to a [100] direction of the crystal, two $S = \pm\frac{1}{2} \leftrightarrow \pm\frac{3}{2}$ fine-structure lines at $H = H_0 \pm 2D + \cdots$, where ellipses represent higher-order terms, from the domains parallel to the [100] and $[\bar{1}00]$ directions and two lines at $H = H_0 \pm D + \cdots$ from the $\{010\}$,$\{0\bar{1}0\}$ and $\{001\}$,$\{00\bar{1}\}$ domains are observed. In addition, the $\pm\frac{1}{2}$ line at $H_0 = h\nu/g\beta$ is of course seen in each case. Such a spectrum is shown in Fig. 2(a). The distances of $4D$ between the outer lines (marked) and $2D$ between the inner lines are accurate to second-order perturbation, an accuracy sufficient for the evaluation of $D_t(T) = b_2^0(T)$.[4]

In the *orthorhombic Amm2 phase,* there are 12 domains with polarization vectors along the $\langle 110 \rangle$ general cubic directions. The Cr^{3+} EPR spectra have their principal

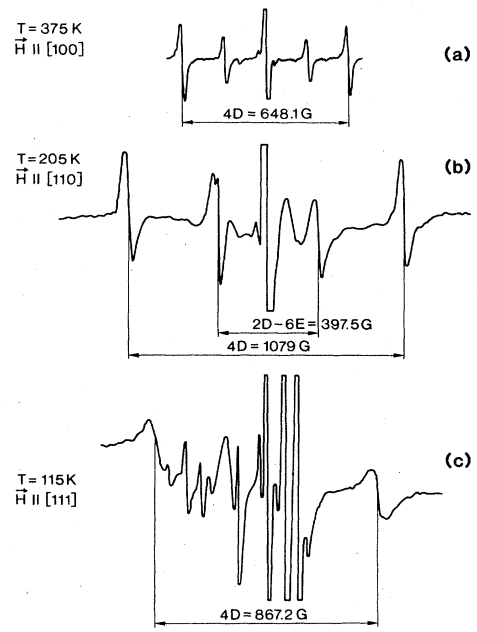

FIG. 2. EPR spectra of Cr^{3+} in $BaTiO_3$, measured at 19.2 GHz. (a) Tetragonal, (b) orthorhombic, (c) rhombohedral phases.

axial vector $\hat{\mathbf{z}}''$ *parallel* to the polarization vector, i.e., along a [110] direction for $\mathbf{P}\|[110]$ plus a smaller orthorhombic component parallel to [001]. Thus, the Hamiltonian is of the form

$$\mathcal{H}=g\beta\mathbf{S}\cdot\mathbf{H}+D_0[S_{z''}^2-\tfrac{1}{3}S(S+1)]+E_0(S_{x''}^2-S_{y''}^2) \quad (2)$$

with $\hat{\mathbf{x}}''\|[1\bar{1}0]$ and $\hat{\mathbf{y}}''\|[001]$.

To first order, the $\pm\frac{1}{2}\leftrightarrow\pm\frac{3}{2}$ fine-structure lines follow the angular dependence[13]

$$\mathcal{H}=H_0\pm D_0(3n^2-1)+3E_0(l^2-m^2)\,, \quad (3)$$

where l, m, and n are the direction cosines of the magnetic field with respect to the x'', y'', and z'' axes. Applying the magnetic field parallel to the cubic [110] direction, two lines at $H_0\pm\frac{1}{2}(D_0+3E_0)$ are observed for the $\{110\}$, $\{1\bar{1}0\}$, $\{\bar{1}10\}$, and $\{\bar{1}\,\bar{1}0\}$ domains, i.e., general $\langle 110\rangle$ directions, and those with general $\langle 101\rangle$ polarization. Furthermore, two lines at $H=H_0\pm(D_0+3E_0)$ occur for the $\{011\}$, $\{0\bar{1}1\}$, $\{01\bar{1}\}$, and $\{0\bar{1}\,\bar{1}\}$ domains, i.e., general $\langle 011\rangle$ directions.

Upon application of the magnetic field H parallel to a pseudocubic [110] direction, six fine-structure lines in addition to the magnetic $\pm\frac{1}{2}$ transition at H_0 are seen; two lines from the $\{110\}$ and $\{\bar{1}\,\bar{1}0\}$ domains at $H=H_0\pm 2D_0+\cdots$; two others at $H=H_0\pm(D_0-3E_0)$ from the domains perpendicular to [110], and two unresolved lines at $H=H_0\pm(D_0+3E_0)/4$ from domains with general $\langle 101\rangle$ polarization. Such a spectrum is displayed in Fig. 2(b). From the data, the values of the D_0 and E_0 parameters and relative signs can be evaluated and cross checked. Figure 3 displays the angular variation of the various fine-structure lines for orientations of H between the [100] and [110] directions as experimentally observed at $T=280$ K, and computed electronically from Eq. (2) with $D_0=185.0\times10^{-4}$ cm^{-1}, $E_0=32.0\times10^{-4}$ cm^{-1}.

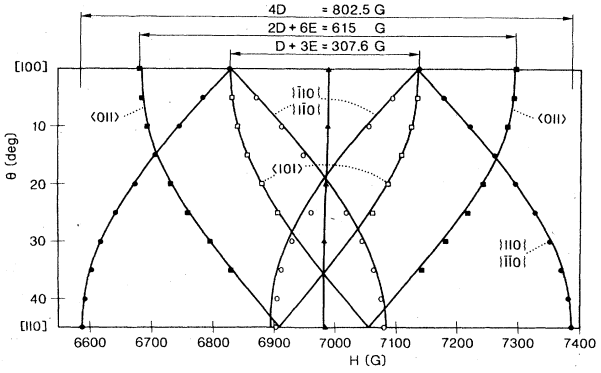

FIG. 3. Angular variation of Cr^{3+} lines in the orthorhombic phase at 280 K.

In the *rhombohedral R 3m phase,* the EPR spectra are again axial and directed along the eight possible trigonal $\langle 111\rangle$ ferroelectric axes. The Hamiltonian describing the spectrum for one domain along $\{111\}$ is

$$\mathcal{H}=g\beta\mathbf{S}\cdot\mathbf{H}+D_r[S_{z'''}^2-\tfrac{1}{3}S(S+1)] \quad (4)$$

with $\hat{\mathbf{z}}'''\|[111]$.

Applying a magnetic field parallel to a [111] direction yields two fine-structure lines at $H=H_0\pm 2D_r$ from the [111] and $(\bar{1}\,\bar{1}\,\bar{1})$ domains, and two other fine-structure lines at $H=H_0\pm\frac{2}{3}D_r$ from the other six symmetry equivalent domains. Such a spectrum is shown in Fig. 2(c). Here, as for the tetragonal case, the value of D_r can be evaluated and double checked for one single spectrum as the distances between each of the two inner and outer lines are $\frac{4}{3}D$ and $4D$, respectively.

C. Temperature dependence of the fine-structure terms

The dependence of the $b_2^m(T)$ spin-Hamiltonian parameters has been measured as a function of temperature in

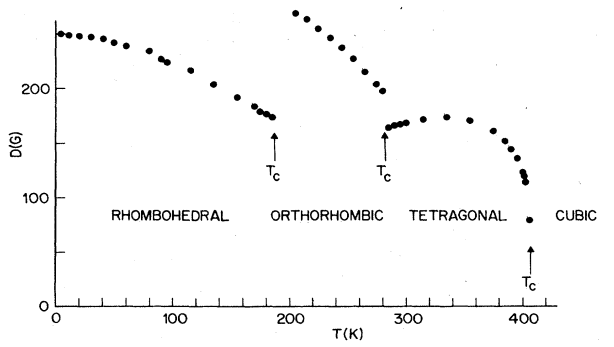

FIG. 4. Temperature dependence of $|D(T)|$ in the three ferroelectric phases of $BaTiO_3$.

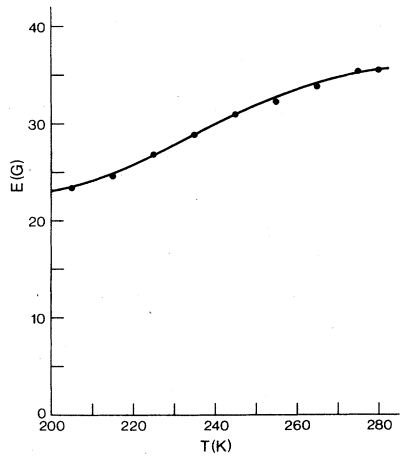

FIG. 5. Variation of parameter $E(T)$ in the orthorhombic phase of Cr^{3+} in $BaTiO_3$.

the three ferroelectric phases down to liquid-helium temperature. This was carried out by recording the spectra as shown in Fig. 2, and evaluating according to the preceding section. The b_2^m values change abruptly at the first-order transitions; their signs in the tetragonal and orthorhombic phases could not be determined. This is in contrast to those of Fe^{3+}, $S=\frac{5}{2}$, which has a positive cubic splitting parameter a relative to which the $b_2^0 \equiv D$ term signs could be evaluated. In Fig. 4 the variation of the $|D|$ terms with temperature is shown. Of interest are the maximum in the tetragonal phase and the marked linear increase in the orthorhombic and trigonal phases upon cooling. The discontinuities at all three first-order transitions are clearly visible. Figure 5 shows the temperature dependence of the $|E(T)|$ term in the orthorhombic phase.

Before concluding this section, we draw attention to the $D_r(T)$ behavior below 50 K in Fig. 4. A leveling off is clearly visible upon approaching 4.2 K, the lowest temperature at which data were taken. In the quantum regime, all parameters have to become temperature independent, therefore, $d[D(T)]/dT=0$ as observed.

III. ANALYSIS OF THE TEMPERATURE DEPENDENCE OF $D(T)$

A. High-temperature behavior

In the temperature dependence of $|D|$ depicted in Fig. 4, there are three unexpected features: A maximum in the tetragonal phase, a larger magnitude in the orthorhombic phase with a marked linear progression in this phase and above 100 K in the trigonal phase. In the latter phase at low temperatures, the polarization is nearly temperature independent.[14] This suggests a large component of $D(T)$ is proportional to T (D^T), at least in this phase above 100 K in addition to one (D^P) that is explicitly dependent on the polarization P. Terms linear in T are well known to occur in axial EPR spectra at higher temperatures owing to thermal fluctuations.[15] Therefore, we use the following ansatz for the analysis. In each ferroelectric phase, there exists an explicit polarization dependence D^P as well as one on temperature D^T,

$$D(T)=D^P+D^T . \tag{5}$$

For D^P, the first two terms of a Taylor-series expansion in P are taken into account, i.e., terms linearly and quadratically proportional to P, and in the range $T>100$ K, D^T was assumed to be proportional to $T-T_0$,

$$D(T)=\alpha_i^{(1)}P(T)+\alpha_i^{(2)}P(T)^2+\beta_i(T-T_0) \tag{6}$$

with $i=t,o,r$ denoting the tetragonal, orthorhombic, and trigonal ferroelectric phases, respectively.

Close to the tetragonal-cubic phase transition, it is difficult to analyze the occurrence of particular terms in Eq. (6). However, using the whole tetragonal range and the measured polarization P below T_c from samples cut from the same boule, a unique fit with

$$\alpha_t^{(1)}=0,\ |\alpha_t^{(2)}|=0.28(3)\ \mathrm{G\,cm^4/\mu C^2},\quad |\beta_t|=0.56(5)\ \mathrm{G/K} \tag{7}$$

could be obtained, see Fig. 6. The sign of β_t is opposite to that of $\alpha_t^{(2)}$, and yields the extremum of $D(T)$. The absolute signs, of course, have so far been undetermined in the analysis. They are fixed in the next section. A really important consequence of the simple assumptions (5) and (6) is that *the slope β_t of D^T in the tetragonal phase is within experimental error the same as $\beta_r=0.61$ in the rhombohedral phase.* We have therefore assumed that the slope of the D^T term in the orthorhombic phase is equal, too,

$$\beta_t=\beta_0=\beta_r=0.58(5)\ \mathrm{G/K}, \tag{8}$$

where the first and last are fixed by experiment. With (8), D^T in (5) is given in all FEP's which allows us to determine D^P in them by subtraction of D^T from the measured $D(T)$. This is also shown in Fig. 6. It should be noted that the data require D^T and D^P to be of the same sign in the orthorhombic and rhombohedral phases.

The absence of a term proportional to $P(T)$, $\alpha_t^{(1)}=0$, in the tetragonal phase indicates Cr^{3+} is centered in the octahedron of $BaTiO_3$ like Fe^{3+} and does not participate in the cooperative polar Ti^{4+} motion of this phase. Therefore, it is likely that Cr^{3+} also remains centered in the orthorhombic and rhombohedral phases, like Fe^{3+}. Furthermore, the magnitude of the polarization P in the orthorhombic and rhombohedral phases is nearly the same as the saturation magnitude in the tetragonal one.[14] Thus it is difficult to imagine a mechanism to drive the Cr^{3+} off center in the orthorhombic or rhombohedral phases if it is centered in the tetragonal phase. Therefore, it is a likely assumption to set $\alpha_0^{(1)}=\alpha_r^{(1)}=0$, but in the next section we shall account for $D_t=\alpha_t^{(2)}P_t^2$, $D_0=\alpha_0^{(2)}P_0^2$, and $D_r=\alpha_r^{(2)}P_r^2$, with the superposition model. An open question remains why T_0 in the D^T term is close to but not coincident with the cubic-to-tetragonal transition T_c. Possibly this is related to the order-disorder character of

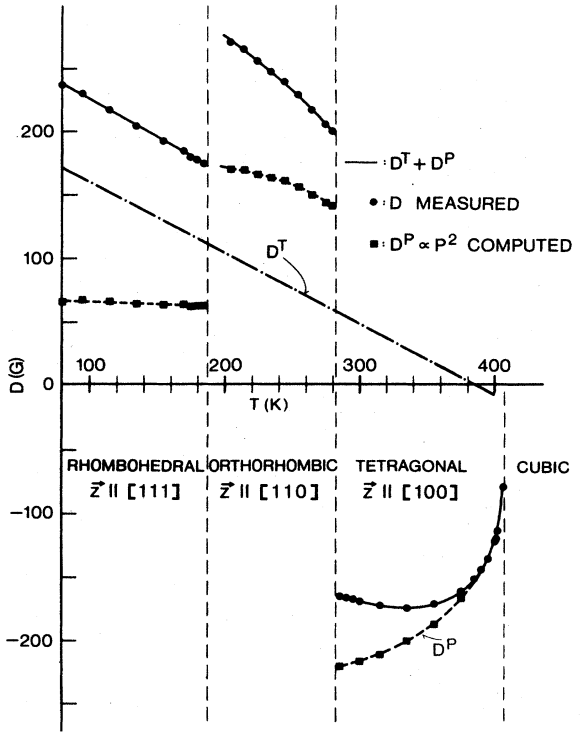

FIG. 6. Analysis of $D(T)$ of Fig. 4 with Eq. (6), and $\alpha_i^{(1)}=0$, $\beta_i=\beta$; $i=t,o,r$.

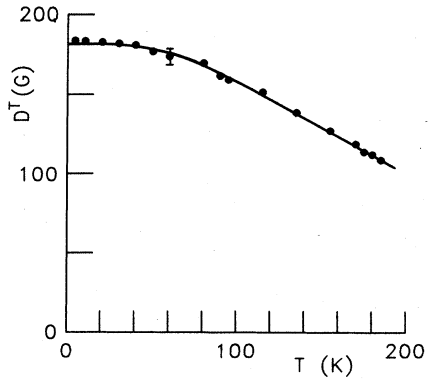

FIG. 7. Temperature variations of D^T for Cr^{3+} in the rhombohedral phase of $BaTiO_3$ (circles) and computed values (line) according to Eq. (10).

the transition,[16] but no mechanism is immediately obvious. Another possibility is the occurrence of an incommensurate phase near T_c, an idea advocated recently by Toledano.[17]

B. Low-temperature behavior

Figure 7 shows the temperature dependence of the quantity $D_r^T=D(T)-\alpha_r^{(2)}P_r^2$ below 200 K. In this region, $P_r(T)$ is temperature independent.[14] Thus, we can ascribe the temperature dependence D^T to the spin-phonon interaction. If interaction with a Debye-phonon spectrum is assumed, then in the long-wavelength limit[15,18]

$$D_r^T=D(0)\left[1-C\frac{T^4}{\Theta_D^4}\int_0^{\Theta_D/T}\frac{x^3}{e^x-1}dx\right], \tag{9}$$

where C is a constant and Θ_D is the Debye temperature.

An alternative model involving a single Einstein oscillator gives

$$D_r^T(T)=D(0)\left\{1-C\left[\coth\left[\frac{\hbar\nu}{2kT}\right]-1\right]\right\}, \tag{10}$$

where $h\nu$ is the energy of the interacting phonon mode. Formulas (9) and (10) are transposed from those used by Blazey *et al.* for the temperature dependence of the hyperfine parameter of anomalous muonium in germanium, and we follow their treatment closely.[18]

The parameters derived for the best fit to the Debye model are

$$\begin{aligned} &D^T(0)=183.0\pm0.6\text{ G}, \\ &C=2.58\pm0.25, \\ &\Theta_D=236.6\pm14.6\text{ K}, \\ &\beta=D(0)\frac{C}{3\Theta_D}=0.67\pm0.12\text{ G/K}. \end{aligned} \tag{11}$$

On the other hand, the parameters providing the best fit to the Einstein oscillator formula (10) are

$$\begin{aligned} &D^T(0)=182.8\pm0.6\text{ G}, C=0.298\pm0.028, \\ &h\nu/2k=84.2\pm5.2\text{ K}, \\ &\beta=D(0)C\frac{2k}{h\nu}=0.65\pm0.10\text{ G/K}. \end{aligned} \tag{12}$$

The agreement between the $T=0$ splitting $D^T(0)$ of both models is, as it should be, very good. The values of β are larger than those from Eq. (8) but still within the experimental limits. The ratio of Θ_D to $h\nu/k$ in Eqs. (11) and (12) amounts to 1.4. This means that either model yields an interaction with low-frequency phonons. Considering that Θ_D for Fe^{3+} in $BaTiO_3$ is 450 K,[19] which is a factor 1.9 larger than Θ_D for Cr^{3+} or a factor 2.7 larger than $h\nu/k$, our data on $D^T(T)$ at low temperatures indicate a local soft-frequency oscillation of the Cr^{3+}. Analysis with the superposition model confirms this, as outlined in the next section.

IV. SUPERPOSITION-MODEL ANALYSIS

The success in analyzing the Fe^{3+} EPR in $BaTiO_3$ with the superposition model[4] and the availability of the $\bar{b}_2(R)$ curves for Cr^{3+} (Ref. 7) was a challenge in trying the model for $BaTiO_3$. The ratio of axial terms $b_2^0(Fe^{3+})/b_2^0(Cr^{3+})=-0.87$ in *trigonal* Al_2O_3 as well as $LaAlO_3$ could be accounted for with the model.[7] In

$BaTiO_3$, the high-temperature phases have *tetragonal* and *orthorhombic* symmetries. The model for Cr^{3+} has not been tried so far for these symmetries. As shown below, it does indeed account quantitatively for the data.

The second-order fine-structure terms in the general spin Hamiltonian $H_F=\sum_{m=-2}^{m=+2} b_2^m O_2^m$, where the b_2^m are constants and the O_2^m are normalized spin operators, can be transformed to axes whereby only the O_2^0 and O_2^2 terms do not vanish, $\mathcal{H}_F=b_2^0[S_z^2-\frac{1}{3}S(S+1)]+\frac{1}{3}b_2^2(S_x^2-S_y^2)$. In the superposition model, the two remaining constants b_2^0 and b_2^2 are evaluated from the contributions of nearest-neighbor ligands owing to their distance and position,

$$b_2^0=\bar{b}_2(R_0)\tfrac{3}{2}\sum_1^n\left[\frac{R_0}{R_i}\right]^{t_2}(\cos^2\Theta_i-\tfrac{1}{3}),$$
$$b_2^2=\bar{b}_2(R_0)\tfrac{3}{2}\sum_1^n\left[\frac{R_0}{R_i}\right]^{t_2}[\sin^2\Theta_i\cos(2\psi_i)]. \quad (13)$$

Here, R_0 is the reference point chosen nominally near the distances R_i between the paramagnetic ion and the ith ligand. Θ_i is the angle between the paramagnetic ion towards the ith ligand and the main EPR axis; ψ_i is the angle between the EPR axis and the projection of the ith ligand coordinate in the xy plane.

The two parameters $\bar{b}_2(R_0)$ and t_2 appearing in Eq. (13), have been evaluated[5] for Cr^{3+} on a Me^{4+}-ion site. In Eq. (13), $\bar{b}_2(R_0)(R_0/R)^{t_2}$ can be replaced by $\bar{b}_2(R)$ as reproduced in Fig. 8. The essential difference for the Cr^{3+} curve as compared to the one for Fe^{3+} is the positive sign and, most importantly, a maximum at $R_m=1.957$ Å.[5] Thus, around R_m, t_2 is small, typically $t_2<1$, whereas $t_2=8\pm1$ for Fe^{3+}. For Cr^{3+}, the exact superposition model formulas[4] may be approximated by those shown in Fig. 9 for the noncubic $BaTiO_3$ phases. From the formulas, one sees that in the tetragonal *and* orthorhombic phases, b_2^0 is proportional to the product $t_2\bar{b}_2$, whereas b_2^2 in the orthorhombic and b_2^0 in the rhombohedral phase are proportional to $\bar{b}_2$. Because t_2 is proportional to the logarithmic derivative of $b_2(R)$ at R, the maximum of $\bar{b}_2$, entails a negative t_2, for $R<R_m$ as found in $SrTiO_3$, whereas for $BaTiO_3$ with $R>R_m$, $t_2>0$ is expected. This is a sensitive test for the model in itself.

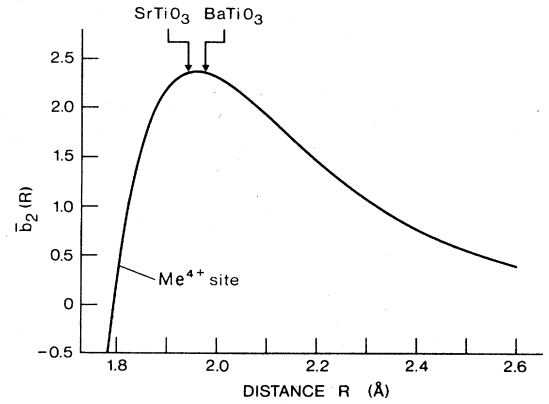

FIG. 8. $\bar{b}(R)$ for Cr^{3+} substitutional for Me^{4+} sites in oxygen octahedral coordinations taken from Ref. 7.

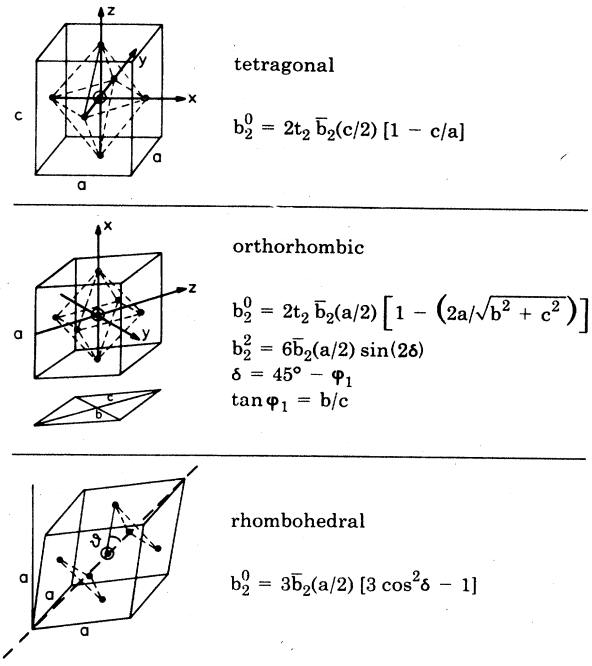

FIG. 9. Superposition-model equations for centered Cr^{3+} in the three ferroelectric phases of $BaTiO_3$.

The axes in Fig. 9 are those observed for Fe^{3+}. The Fe^{3+} principal magnetic axis in the orthorhombic phase is along [001], *perpendicular* to the [110] polarization axes, but for Cr^{3+} it is observed *along* [110]. It is easy to go from the former to the latter orientation of axes in an orthorhombic fine-structure term of the form

$$\mathbf{S}\cdot\vec{\mathbf{D}}\cdot\mathbf{S}=D_{xx}S_x^2+D_{yy}S_y^2+D_{zz}S_z^2.$$

Setting as usual the trace $D_{xx}+D_{yy}+D_{zz}=0$ and choosing the principal axes along z,[13]

$$\mathbf{S}\cdot\vec{\mathbf{D}}\cdot\mathbf{S}=b_2^0(S_z^2-\tfrac{1}{3}S^2)+\tfrac{1}{3}b_2^2(S_x^2-S_y^2)$$

with

$$b_2^0\equiv\tfrac{3}{2}D_{zz},\quad b_2^2=\tfrac{3}{2}(D_{xx}-D_{yy}) \quad (14)$$

and $D=\frac{1}{2}(b_2^2-b_2^0)$, $E=-\frac{1}{2}(\frac{1}{3}b_2^2+b_2^0)$,

$$\mathbf{S}\cdot\vec{\mathbf{D}}\cdot\mathbf{S}=D(S_x^2-\tfrac{1}{3}S^2)+E(S_y^2-S_z^2)$$

with $\hat{\mathbf{x}}\|[110]$, $\hat{\mathbf{y}}\|[\bar{1}10]$, $\hat{\mathbf{z}}\|[001]$. From the above, for positive b_2^2 and b_2^0, the principal axis will lie along the polarization axis [110], if $\frac{1}{3}b_2^2>b_2^0$ in the superposition-model calculation. For $\frac{1}{3}b_2^2<b_2^0$, the axis is as observed and calculated for Fe^{3+}, i.e., [001].

We now analyze the D^P terms in the tetragonal and

orthorhombic phases together. In the former, $D_t^P \equiv b_2^0$, and in the latter, $D_0^P = \frac{1}{2}(b_2^2 - b_2^0)$ from Eq. (13). Because in the orthorhombic phase the main axis is along $\hat{\mathbf{x}} \| [110]$, $b_2^2 > |b_2^0|$. In the orthorhombic phase, $b_2^2 = 6\bar{b}_2 \sin(2\delta)$ from Fig. 9 and Ref. 4, and $\sin(2\delta) = \sin[\pi/4 - \arctan(b/c)] = 0.0656$, a positive quantity. Thus $b_2^2 = 6\bar{b}_2 \sin(2\delta) > 0$. From Fig. 6, we see that b_2^0 in the tetragonal and orthorhombic phases must have opposite signs, therefore in the tetragonal phase, $D_T^P = b_2^0(T) < 0$ as in Fig. 6. D_T^P obtained from Fig. 6 amounts to 215 G or 199×10^{-4} cm^{-1}. At 300 K with $c/a = 1.0110$ and the formula from Fig. 9, we obtain $t_2 \bar{b}_2 = -0.9045$. $\bar{b}_2(c/2)$ varies very little near R_m, and we use $\bar{b}_2 = +2.40$ cm^1; *thus* $t_2 = -0.38 \pm 0.04$.

With t_2 fixed from the D^T in the tetragonal phase, there is no adjustable quantity to determine the D_0^P and E_0^P spin-Hamiltonian parameters in the orthorhombic phase. Because Cr^{3+} is centered, $D^T = \alpha_0^{(2)} P^2(T)$ with little T dependence and it is only necessary to calculate one point using the equations given in Fig. 9. They are compared in Table I, to experiment at $T = 280$ K, i.e., just below the tetragonal orthorhombic phase transition. There, $D^P = 133$ G from Fig. 6 or 123×10^{-4} cm^{-1}. The quantity computed is 115×10^{-4} cm^{-1} in excellent agreement. Note that b_2^2 and b_2^0 contribute additionally.

b_2^2 and b_2^0 are both positive in the orthorhombic phase. Consequently, $E_0^P = -\frac{1}{2}(\frac{1}{3} b_2^2 + b_2^0)$ is definitely negative near -101×10^{-4} cm^{-1}, whereas the measured quantity $E_0 = +32 \times 10^{-4}$ cm^{-1}. Referring to Eq. (5) for $D(T)$, $E_0(T)$ and E_0^P also have to be related by

$$E_0(T) = E_0^P + E_0^T , \tag{15}$$

i.e., a term due to thermal fluctuations. For it from Eq. (15), $E_0^T = (32 \times 10^{-4} - E_0^P) \approx 133 \times 10^{-4}$ cm^{-1}. To arrive at the latter number, we have used the computed quantity of E_0^P to which we attach a relatively high degree of confidence because the agreement between calculated and observed D_0^P is so good. The E_0^T fluctuation term we deduced is comparable to D_0^T, which varies between 70×10^{-4} cm^{-1} and 110×10^{-4} cm^{-1} in the orthorhombic phase. This is quite a satisfactory result because we expect the local thermal fluctuations of the Cr^{3+} in the octahedral cage to be comparable in the [001] and [110] directions.

For Fe^{3+}, a one-parameter model was used to account for the b_2^m values. In this model, the Fe^{3+} was displaced by an amount Δd along the ferroelectric axes from the crystallographic Ti^{4+} site, d being the average Ti-O distance. By using the same parameter values Δ for Cr^{3+} as those in Table II of Ref. 4 for Fe^{3+}, i.e., assuming the average Cr^{3+} coordinate to be the same as Fe^{3+}, values given in column 2 of Table I are obtained. They are close to the ones observed. This also pertains to the rhombohedral phase where the observed D_r^P values of Fe^{3+} and Cr^{3+} calculated from the centered model both deviate by about a factor of 4 to 5. This could mean that both ions lie very slightly off center along [111] in that phase. All in all, the agreement between experimental second-order Hamiltonian values, especially the $D(T)$, calculated from the $\bar{b}_2(R)$ curve of Müller and Berlinger is really satisfactory.

The t_2 exponent of $+0.38$ explaining the Hamiltonian parameters D^T in the tetragonal and orthorhombic phases in $BaTiO_3$ is of the same size as obtained for $SrTiO_3$ but of opposite sign. For the latter perovskite, $t_2 = -0.36$. Referring to Fig. 8 and our earlier discussion, this proves that $R > R_m$ in $BaTiO_3$, and the difference between R_m and R is about the same as in $SrTiO_3$ but in the opposite direction from R_m as marked on the figure, $|R - R_m| \simeq 0.15$ Å. On the other hand, where the oxygens surrounding the Cr^{3+} at their intrinsic distance $\bar{R} \simeq 2.003$ Å with $R_m = 1.967$ Å, $(R - R_m) = 0.036$ Å. Therefore, our data imply an effective inward relaxation of 0.021 Å. However, the size of Cr^{3+} is very close to the one of Ti^{4+} and Fe^{3+}.[7] Because the charge misfit is already included in the $\bar{b}_2(R)$ curve,[4] there must be an additional mechanism to cause this effective inward relaxation. The only possibility is the large thermal fluctuations of the Cr^{3+} as exemplified by the low Einstein or Debye energies obtained from low-temperature behavior and its analysis in Sec. III B and Fig. 7. These fluctuations result in an effectively reduced Cr^{3+}-O^{2-} distance.

V. CONCLUSIONS

The present EPR experiments and their analysis are satisfactory in two ways: They give insight into the local

TABLE I. Comparison of Cr^{3+} EPR data in the three FEP's of $BaTiO_3$ with two models on the basis of the superposition model.

Phase	Experimental EPR data (10^{-4} cm^{-1})	One-parameter model[a] (10^{-4} cm^{-1})	Centered model[b] (10^{-4} cm^{-1})
Tetragonal	$D_t^P = -199(2)$ $\mathrm{sgn} D_t^P = -\mathrm{sgn} D_0^P$	$D_t^P = -213(36)$	$D_t^P = -199$
Orthorhombic	$D_0^P = +123(1)$ $E_0^P = +32 - E^T$	$D_0^P = +108(18)$ $E_0^P = -98(17)$	$D_0^P = +115(19)$ $E_0^P = -101(17)$
Rhombohedral	$D_r^P = +60(1)$	$D_r^P = +83(14)$	$D_r^P = +299(39)$

[a]Deviation Δ the same as for Fe^{3+} in Ref. 7.
[b]D_t^P used to determine $|t_2|$.

behavior of Cr^{3+} in $BaTiO_3$ on Ti^{4+} sites, and at the same time confirm the superposition model for Cr^{3+} in an oxygen octahedral environment as published recently by Müller and Berlinger.[7]

The work presented proves that the Cr^{3+} remains centered in its oxygen cage in the three ferroelectric $BaTiO_3$ phases, like the Fe^{3+}. However, its local potential is considerably flatter than that of Fe^{3+}, with large ionic fluctuations of the order of 0.02 Å larger than Fe^{3+} and a local Debye energy of 236.6 K.

The superposition model for Cr^{3+} accounts for the second-order spin-Hamiltonian parameters as well as those for Fe^{3+}, despite other crystal-field main-axis orientations in the orthorhombic phase. Furthermore, the data of Cr^{3+} in $BaTiO_3$ prove the existence of a maximum in the superposition-model $\bar{b}_2(R)$ parameter, near the $R=1.96$ Å recently inferred from EPR stress experiments of Cr^{3+} in cubic $SrTiO_3$.[7]

ACKNOWLEDGMENTS

The authors would like to thank Professor W. Kündig for the Debye and Einstein oscillator fits in Fig. 7, and Dr. K. W. Blazey and Dr. E. Siegel for a critical reading of the manuscript.

[1]E. Siegel and K. A. Müller, Phys. Rev. B **20**, 3587 (1979).
[2]A. W. Hornig, R. C. Rempel, and H. E. Weaver, J. Phys. Chem. Solids **10**, 1 (1959).
[3]T. Sakudo, J. Phys. Soc. Jpn. **18**, 1626 (1963); T. Sakudo and H. Unoki, J. Phys. Soc. Jpn. **19**, 2109 (1964).
[4]E. Siegel and K. A. Müller, Phys. Rev. B **19**, 109 (1979).
[5]M. J. L. Sangster, J. Phys. C **14**, 2889 (1981).
[6]H. D. Megaw, *Crystal Structures: A Working Approach* (Saunders, Philadelphia, 1973), p. 26.
[7]K. A. Müller and W. Berlinger, J. Phys. C **16**, 6861 (1983).
[8]V. Belruss, J. Kalnajs, and A. Linz, Mater. Res. Bull. **C**, 899 (1971).
[9]J. Albers, First European Conference on Crystal Growth, Zurich, 1976 (unpublished), p. 150.
[10]W. Berlinger and K. A. Müller, Rev. Sci. Instrum. **48**, 1161 (1977).
[11]W. Low, Phys. Rev. **105**, 801 (1957).
[12]K. A. Müller, Arch. Sci. (Genève) **11**, 150 (1958).
[13]G. E. Pake and T. L. Estle, *The Physical Principles of Electron Paramagnetic Resonance, Frontiers in Physics* (Benjamin, New York, 1973).
[14]W. I. Merz, Phys. Rev. **95**, 690 (1954); F. Jona and G. Shirane, *Ferroelectric Crystals* (Pergamon, New York, 1962). The measured polarizations P of the crystals used in our experiments were 295 K (tetragonal) 0.288 C/m^2; 225 K (orthorhombic) 0.337 C/m^2; 125 K (rhombohedral) 0.361 C/m^2 [W. Kuhn (private communication)].
[15]K. N. Shrivastava, Phys. Rep. **20C**, 137 (1975).
[16]K. A. Müller, Y. Luspin, J. L. Servoin, and F. Gervais, J. Phys. (Paris) Lett. **43**, L537 (1982).
[17]P. Toledano (private communication).
[18]K. W. Blazey, T. L. Estle, E. Holzschuh, W. Odermatt, and B. D. Patterson, Phys. Rev. B **27**, 15 (1983).
[19]V. G. Bhide and M. S. Multani, Phys. Rev. A **139**, 1983 (1965).